Application of PML absorbing boundary condition to aeroacoustic problems with an oblique mean flow

Sarah A. Parrish* and Fang Q. Hu †

Old Dominion University, Norfolk, Virginia, 23529, United States

For the case of uniform mean flow in an arbitrary direction, Perfectly Matched Layer (PML) absorbing boundary conditions are presented for both the linearized and nonlinear Euler equations. Perfectly matched side layers and stable corner layers are proposed. Stability issues are investigated by examining the dispersion relations of linear waves. For increased efficiency, a pseudo mean flow is included in the derivation of the PML equations for the nonlinear case. Numerical examples are given to support the validity of the proposed equations. Specifically, the linear PML formulation is tested for the case of entropy and vorticity waves traveling with oblique mean flow. The nonlinear formulation is tested with an isentropic vortex moving diagonally with constant velocity.

I. Introduction

The use of a nonreflecting boundary condition is imperative when considering aeroacoustic problems with open physical domains, as reflections off numerical boundaries can compromise the accuracy of the solution within the computational domain. As the accuracy of spatial and temporal discretizations increases, the need for greater accuracy at the boundaries increases accordingly. The Perfectly Matched Layer (PML) technique has proven effective in eliminating boundary reflections with sufficient accuracy. Originally proposed for the numerical solution of Maxwell equations in [4], the PML technique has been extended in recent studies to the governing equations of Computational Fluid Dynamics (CFD) and Computational Aeroacoustics (CAA). PML has been developed for the linearized Euler equations with a constant or non-constant mean flow and, most recently, for the nonlinear Euler and Navier-Stokes equations [6]-[13].

Most of the work done has been specific to mean or background flow that is perpendicular to a boundary. There are very few works where a mean flow not perpendicular to the boundary was considered. In [1], the PML for truncating the domain in x direction was given where the mean flow Mach number M_x and M_y can both be nonzero. However, the equations for the corner layers were not derived. In [5], only the acoustic waves were considered for an oblique mean flow. In [13], a new formulation of PML for the linearized Euler equations based on the Smith-factorizations was given in which the direction of mean flow can be arbitrary. Whether this approach can be extended to nonlinear equations remains to be seen.

The goal of this paper is to apply the PML technique to the more general case of mean flow in an arbitrary direction. Such a formulation can be useful in many practical applications, such as when an aircraft travels at a nonzero angle of attack, when a slant boundary is present, or when a transformed coordinate is used for nonlinear problems. For instance, in transformed coordinates (ξ, η, ζ), the governing equation takes the form

$$\frac{\partial}{\partial t}\left(\frac{\mathbf{u}}{J}\right) + \frac{\partial}{\partial \xi}\left(\frac{\xi_x \mathbf{E} + \xi_y \mathbf{F} + \xi_z \mathbf{G}}{J}\right) + \frac{\partial}{\partial \eta}\left(\frac{\eta_x \mathbf{E} + \eta_y \mathbf{F} + \eta_z \mathbf{G}}{J}\right) + \frac{\partial}{\partial \zeta}\left(\frac{\zeta_x \mathbf{E} + \zeta_y \mathbf{F} + \zeta_z \mathbf{G}}{J}\right) = 0 \quad (1)$$

where $\mathbf{E}$, $\mathbf{F}$ and $\mathbf{G}$ are the flux vectors in (x, y, z) coordinates and J is the Jacobian of the transformation. In particular, the transformed velocity becomes

$$U = \xi_x u + \xi_y v + \xi_z w,\ V = \eta_x u + \eta_y v + \eta_z w,\ W = \zeta_x u + \zeta_y v + \zeta_z w \quad (2)$$

*Graduate research assistant, Department of Mathematics and Statistics, Norfolk, Virginia.

†Professor, Department of Mathematics and Statistics, Norfolk, Virginia, AIAA associate fellow.

Copyright © 2007 by F. Q. Hu. Published by the American Institute of Aeronautics and Astronautics, Inc., with permission.

Therefore, the mean velocity will not be necessarily aligned with transformed coordinates, even if it is aligned with the original Cartesian coordinates.

As we will see in this paper, the difficulty in developing PML for a mean flow that is oblique to the boundary lies in the fact that, in addition to the acoustic waves, the vorticity and entropy waves also become inconsistent in the phase and group velocities. Recent studies on the PML for fluid dynamics equations have shown that it is important to apply a proper space-time transformation to the governing equations so that the phase and group velocities are consistent for all waves before the PML technique can be applied. It seems however there is no proper space-time transformation available to correct both type of waves simultaneously before the application of the PML technique. In the current approach, we will develop PML for the side and corner layers separately. Linear stability analysis will be performed to ensure the dynamic stability of the proposed equations.

The next section examines first the dispersion relations of linear waves. Following, the PML equations for the linearized and nonlinear Euler equations are given. Finally, numerical results are given to show the effectiveness of the proposed equations.

II. Dispersion relations of linear waves

Figure 1 shows a schematic diagram of a truncated computational domain. Absorbing boundary conditions are needed at the x- and y-layers and the corner layers. Recently, a new PML formulation was given in [13] for the linearized Euler equations based on Smith-factorizations. This approach, however, does not seem to be easily extendable to nonlinear Euler and Navier-Stokes equations. In [1], a situation without top and bottom y-layers was considered. It was suggested that for the x-layers alone, the PML derived for $M_y = 0$ can still be used when the time derivative was replaced with a material derivative based on the nonzero transverse velocity M_y. Such a treatment, however, will not be complete if a top or bottom y-layer is present, giving rise to corner layers. Indeed, although the part of the mean flow transverse to the layer interface can be easily eliminated by using a moving frame along the same direction, the difficulty as we will show next is that no such treatment is possible for the corner layers.

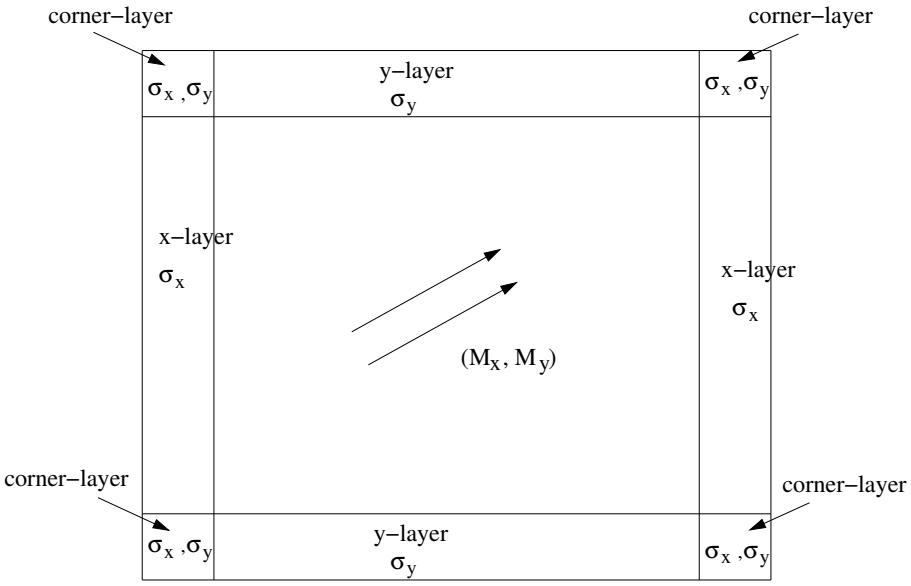

Figure 1. Schematics of absorbing layers at the vertical, horizontal and corner regions, with nonzero absorption coefficients indicated.

To illustrate the main difficulties in constructing a PML for a mean flow of arbitrary direction, consider the two-dimensional linearized Euler equation with a mean flow of Mach number (M_x, M_y),

$$\frac{\partial \mathbf{u}}{\partial t} + \mathbf{A}\frac{\partial \mathbf{u}}{\partial x} + \mathbf{B}\frac{\mathbf{u}}{\partial y} = 0, \tag{3}$$

$$\mathbf{u} = \begin{pmatrix} \rho \\ u \\ v \\ p \end{pmatrix}, \ \mathbf{A} = \begin{pmatrix} M_x & 1 & 0 & 0 \\ 0 & M_x & 0 & 1 \\ 0 & 0 & M_x & 0 \\ 0 & 1 & 0 & M_x \end{pmatrix}, \ \mathbf{B} = \begin{pmatrix} M_y & 0 & 1 & 0 \\ 0 & M_y & 0 & 0 \\ 0 & 0 & M_y & 1 \\ 0 & 0 & 1 & M_y \end{pmatrix} \tag{4}$$

where ρ is the density, u and v are velocity components, and p is the pressure.

The dispersion relations of all linear waves for (3) are well-known, i.e.,

$$(\omega - M_x k_x - M_y k_y)^2 - {k_x}^2 - {k_y}^2 = 0 \tag{5}$$

for the acoustic waves and

$$\omega - M_x k_x - M_y k_y = 0 \tag{6}$$

for the vorticity and entropy waves. They are illustrated in Figure 2.

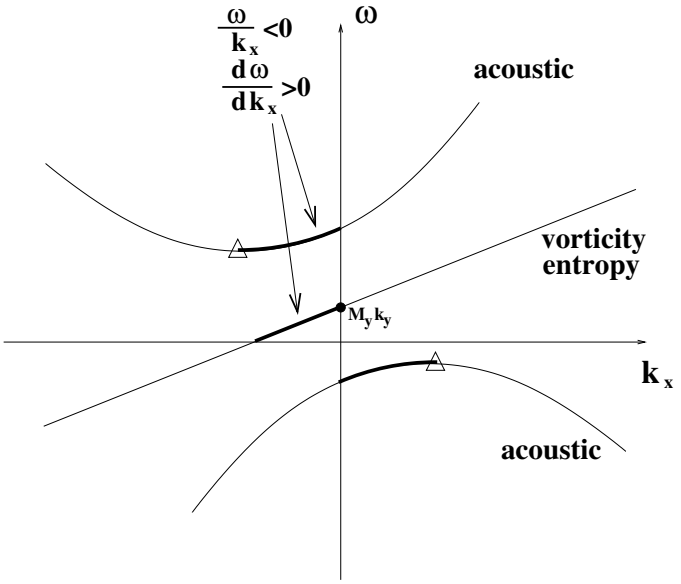

Figure 2. Schematics of the dispersion relations for the acoustic, vorticity and entropy waves with mean flow Mach number (M_x, M_y). Dark lines indicate waves with inconsistent phase and group velocities.

As shown in Figure 2, with nonzero transverse velocity component M_y, both types of dispersion relations support waves with inconsistent signs for the phase and group velocities, where the group velocity is positive while the phase velocity is negative. It has been recognized in recent studies that the PML technique will lead to numerical instability if the inconsistency in the phase and group velocities was not removed by a proper space-time transformation or other means, before applying the PML complex change of variable in the derivation process. With both types of waves having inconsistent phase and group velocities, a single linear space-time transformation, as employed in recent PML studies [2]-[10], will not be sufficient.

III. Absorbing boundary condition for the linearized Euler equations

We will first consider the x- and y-layers separately, and then form stable equations for the corner layer.

To construct vertical x-layers, we introduce a moving frame so that the mean flow is stationary in the vertical direction, similar to the approach used in [1]. Let

$$\bar{y} = y - M_y t \tag{7}$$

which gives

$$\frac{\partial}{\partial y} = \frac{\partial}{\partial \bar{y}}, \ \frac{\partial}{\partial t} = \frac{\partial}{\partial t} - M_y \frac{\partial}{\partial \bar{y}} \tag{8}$$

Then, the Euler equations in x, $\bar{y}$, and t become

$$\frac{\partial \mathbf{u}}{\partial t} - M_y \frac{\partial \mathbf{u}}{\partial \bar{y}} + \mathbf{A}\frac{\partial \mathbf{u}}{\partial x} + \mathbf{B}\frac{\partial \mathbf{u}}{\partial \bar{y}} = 0 \tag{9}$$

or

$$\frac{\partial \mathbf{u}}{\partial t} + \mathbf{A}\frac{\partial \mathbf{u}}{\partial x} + \mathbf{B_0}\frac{\partial \mathbf{u}}{\partial \bar{y}} = 0 \tag{10}$$

where

$$\mathbf{B_0} = \mathbf{B} - M_y \mathbf{I} \tag{11}$$

Therefore, the stable PML for (10) will be the same as that of no vertical mean flow component, as given in [9], namely,

$$\frac{\partial \mathbf{u}}{\partial t} + \mathbf{A}\frac{\partial \mathbf{u}}{\partial x} + \mathbf{B_0}\frac{\partial \mathbf{u}}{\partial \bar{y}} + \sigma_x \mathbf{B_0}\frac{\partial \mathbf{q_1}}{\partial \bar{y}} + \sigma_x \mathbf{u} + \sigma_x \beta_x \mathbf{A}\mathbf{u} = 0 \tag{12}$$

$$\frac{\partial \mathbf{q_1}}{\partial t} = \mathbf{u} \tag{13}$$

where

$$\beta_x = \frac{M_x}{1 - M_x^2} \tag{14}$$

Because the moving-frame transformation (7) does not affect the location of the Euler/PML interface, which is vertical, the above gives a valid x-layer. After rewriting the above in the original physical coordinates x, y, and t, we get the following stable PML x-layer:

$$\frac{\partial \mathbf{u}}{\partial t} + \mathbf{A}\frac{\partial \mathbf{u}}{\partial x} + \mathbf{B}\frac{\partial \mathbf{u}}{\partial y} + \sigma_x \mathbf{B_0}\frac{\partial \mathbf{q_1}}{\partial y} + \sigma_x \mathbf{u} + \sigma_x \beta_x \mathbf{A}\mathbf{u} = 0 \tag{15}$$

$$\frac{\partial \mathbf{q_1}}{\partial t} + M_y \frac{\partial \mathbf{q_1}}{\partial y} = \mathbf{u} \tag{16}$$

Equations (15)-(16) should be equivalent to the PML given in [1]. Similarly, we get the stable PML y-layer:

$$\frac{\partial \mathbf{u}}{\partial t} + \mathbf{A}\frac{\partial \mathbf{u}}{\partial x} + \mathbf{B}\frac{\partial \mathbf{u}}{\partial y} + \sigma_y \mathbf{A_0}\frac{\partial \mathbf{q_2}}{\partial x} + \sigma_y \mathbf{u} + \sigma_y \beta_y \mathbf{B}\mathbf{u} = 0 \tag{17}$$

$$\frac{\partial \mathbf{q_2}}{\partial t} + M_x \frac{\partial \mathbf{q_2}}{\partial x} = \mathbf{u} \tag{18}$$

where

$$\beta_y = \frac{M_y}{1 - M_y^2} \tag{19}$$

Note that $\mathbf{A_0}$ and $\mathbf{B_0}$ are the reduced matrices of $\mathbf{A}$ and $\mathbf{B}$ without the mean flow. The parameters β_x and β_y are necessary for the stability of the layer [9]. The absorption coefficients σ_x and σ_y are positive functions of x and y, respectively.

The remaining issue is the construction of equations for the corner layers where both σ_x and σ_y are nonzero. A study for a corner layer based on a combination of the two layer equations (15)-(18) leads to the following corner equations:

$$\frac{\partial \mathbf{u}}{\partial t} + \mathbf{A}\frac{\partial \mathbf{u}}{\partial x} + \mathbf{B}\frac{\partial \mathbf{u}}{\partial y} + \sigma_y \mathbf{A_0}\frac{\partial \mathbf{q_2}}{\partial x} + \sigma_x \mathbf{B_0}\frac{\partial \mathbf{q_1}}{\partial y} + (\sigma_x + \sigma_y)\mathbf{u} + \sigma_x \beta_x \mathbf{A}\mathbf{u} + \sigma_y \beta_y \mathbf{B}\mathbf{u} = 0 \tag{20}$$

$$\frac{\partial \mathbf{q_1}}{\partial t} + M_y \frac{\partial \mathbf{q_1}}{\partial y} + \sigma_y \mathbf{q_1} = \mathbf{u} \tag{21}$$

$$\frac{\partial \mathbf{q_2}}{\partial t} + M_x \frac{\partial \mathbf{q_2}}{\partial x} + \sigma_x \mathbf{q_2} = \mathbf{u} \tag{22}$$

Equation (20) results from a simple combination of (15) and (17). One feature of (20)-(22) is that they automatically reduce to the x- and y-layer equations (15)-(18), when σ_y and σ_x are zero, respectively. For stability, modifications have been made to the equations for $\mathbf{q_1}$ and $\mathbf{q_2}$, with the addition of $\sigma_x \mathbf{q}_1$ and $\sigma_y \mathbf{q}_2$ terms to the left hand sides of (21) and (22), respectively. As we will see next, the corner equations as given by (20)-(22) are stable for all subsonic Mach numbers (M_x, M_y).

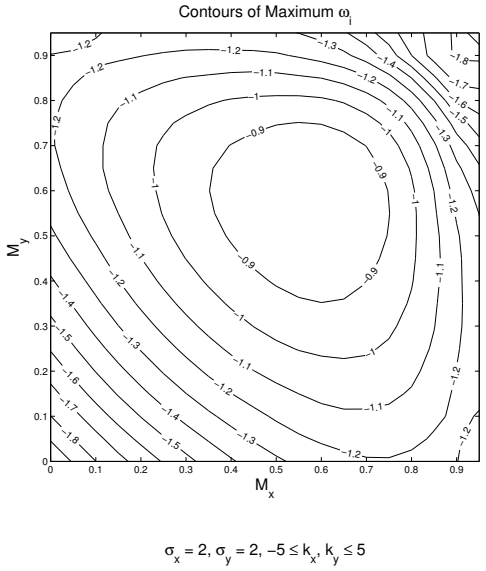

Figure 3. Contours of maximum imaginary part of ω for $\sigma_x = \sigma_y = 2$.

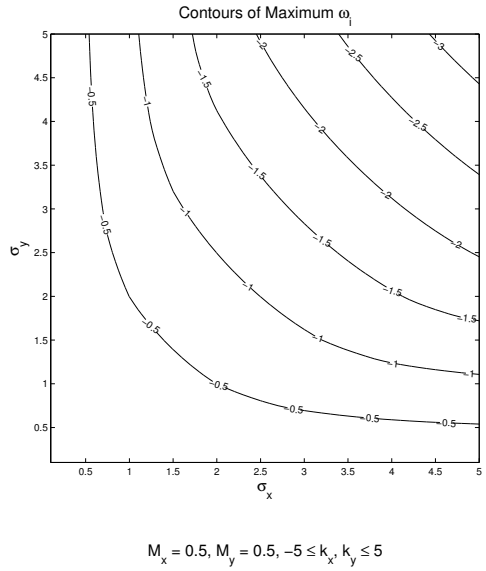

Figure 4. Contours of maximum imaginary part of ω for $M_x = M_y = 0.5$

By substituting

$$\begin{pmatrix} \mathbf{u} \\ \mathbf{q_1} \\ \mathbf{q_2} \end{pmatrix} = e^{i(k_x x + k_y y - \omega t)} \begin{pmatrix} \hat{\mathbf{u}} \\ \hat{\mathbf{q_1}} \\ \hat{\mathbf{q_2}} \end{pmatrix} \tag{23}$$

into (20)-(22) and assuming σ_x and σ_y to be constants, an eigenvalue problem is formed for ω with given values of k_x and k_y. Existence of any eigenvalue ω with a positive imaginary part will indicate instability. On the other hand, the system is dynamically stable if all eigenvalues have a nonpositive imaginary part. In Figures 3 and 4, the results of the stability analysis for (20)-(22) are shown. We plot in Figure 3 the contours of maximum ω_i, the imaginary part of ω, for $0 \le M_x \le 0.95$, $0 \le M_y \le 0.95$, $|k_x| \le 5$, $|k_y| \le 5$, with fixed values $\sigma_x = \sigma_y = 2$. In Figure 4, we show the contours of maximum ω_i for fixed Mach numbers $M_x = M_y = 0.5$ and $0 \le \sigma_x \le 5$, $0 \le \sigma_y \le 5$, $|k_x| \le 5$, $|k_y| \le 5$. We see that the imaginary part of ω for all eigenvalues is negative for the range of absorption coefficients considered. This indicates that the proposed corner equations are stable.

IV. Absorbing boundary condition for the nonlinear Euler equations

We will use a similar approach in formulating a PML equation for the nonlinear Euler equations, considering x- and y-layers individually, then constructing stable corner layers. For easy implementation, the Euler equations are kept in conservation form:

$$\frac{\partial \mathbf{u}}{\partial t} + \frac{\partial \mathbf{F_1}(\mathbf{u})}{\partial x} + \frac{\partial \mathbf{F_2}(\mathbf{u})}{\partial y} = 0 \tag{24}$$

with

$$\mathbf{u} = \begin{pmatrix} \rho \\ \rho u \\ \rho v \\ \rho e \end{pmatrix}, \ \mathbf{F_1} = \begin{pmatrix} \rho u \\ \rho u^2 + p \\ \rho uv \\ \rho hu \end{pmatrix}, \ \mathbf{F_2} = \begin{pmatrix} \rho v \\ \rho uv \\ \rho v^2 + p \\ \rho hv \end{pmatrix} \tag{25}$$

and

$$h = e + \frac{p}{\rho}, \ p = (\gamma - 1)\rho \left(e - \frac{u^2 + v^2}{2} \right) \tag{26}$$

where ρ is the density, u and v are components of velocity, p is the pressure, and e is the energy. Assume a background flow is moving with constant velocity (U_0, V_0).

We begin by partitioning the solution inside the PML domain into two parts as follows:

$$\mathbf{u} = \bar{\mathbf{u}}_\mathbf{p} + \mathbf{u}' \tag{27}$$

where $\bar{\mathbf{u}}_\mathbf{p}$ is the time-independent pseudo mean flow which satisfies the steady Euler equation

$$\frac{\partial \mathbf{F_1}(\bar{\mathbf{u}}_\mathbf{p})}{\partial x} + \frac{\partial \mathbf{F_2}(\bar{\mathbf{u}}_\mathbf{p})}{\partial y} = 0 \tag{28}$$

For the present case, $\bar{\mathbf{u}}_\mathbf{p} = [\rho_0, \rho_0 U_0, \rho_0 V_0, \rho_0 e_0]$. The equation for $\mathbf{u}'$ then becomes

$$\frac{\partial \mathbf{u}'}{\partial t} + \frac{\partial [\mathbf{F_1} - \bar{\mathbf{F}}_\mathbf{1}]}{\partial x} + \frac{\partial [\mathbf{F_2} - \bar{\mathbf{F}}_\mathbf{2}]}{\partial y} = 0 \tag{29}$$

where the shorthand notations $\mathbf{F_1} = \mathbf{F_1}(\mathbf{u})$, $\bar{\mathbf{F}}_\mathbf{1} = \mathbf{F_1}(\bar{\mathbf{u}}_\mathbf{p})$, $\mathbf{F_2} = \mathbf{F_2}(\mathbf{u})$, and $\bar{\mathbf{F}}_\mathbf{2} = \mathbf{F_2}(\bar{\mathbf{u}}_\mathbf{p})$ have been used. We will derive the equations that absorb $\mathbf{u}'$.

To construct the x-layer equations, we now introduce a moving-frame change of variable

$$\bar{y} = y - V_0 t \tag{30}$$

which gives

$$\frac{\partial \mathbf{u}'}{\partial t} + \frac{\partial[\mathbf{F_1} - \bar{\mathbf{F}}_\mathbf{1}]}{\partial x} + \frac{\partial[\mathbf{F_2} - \bar{\mathbf{F}}_\mathbf{2} - \mathrm{V}_0\mathbf{u}']}{\partial \bar{y}} = 0 \tag{31}$$

With the moving-frame, the vertical flow is stationary, so the PML equations are the same as those given in [12], which become

$$\frac{\partial \mathbf{u}'}{\partial t} + \frac{\partial[\mathbf{F_1} - \bar{\mathbf{F}}_\mathbf{1}]}{\partial x} + \frac{\partial[\mathbf{F_2} - \bar{\mathbf{F}}_\mathbf{2} - \mathbf{V_0}\mathbf{u}']}{\partial \bar{y}} + \sigma_x \mathbf{q_1} + \sigma_x \beta_x [\mathbf{F_1} - \bar{\mathbf{F}}_\mathbf{1}] = 0 \tag{32}$$

$$\frac{\partial \mathbf{q_1}}{\partial t} + \frac{\partial[\mathbf{F_1} - \bar{\mathbf{F}}_\mathbf{1}]}{\partial x} + \sigma_x \mathbf{q_1} + \sigma_x \beta_x [\mathbf{F_1} - \bar{\mathbf{F}}_\mathbf{1}] = 0 \tag{33}$$

where

$$\beta_x = \frac{U_0}{1 - U_0^2} \tag{34}$$

Changing back to the original time and space coordinates, we arrive at the x-layer equations:

$$\frac{\partial \mathbf{u}}{\partial t} + \frac{\partial[\mathbf{F_1} - \bar{\mathbf{F}}_\mathbf{1}]}{\partial x} + \frac{\partial[\mathbf{F_2} - \bar{\mathbf{F}}_\mathbf{2}]}{\partial y} + \sigma_x \mathbf{q_1} + \sigma_x \beta_x [\mathbf{F_1} - \bar{\mathbf{F}}_\mathbf{1}] = 0 \tag{35}$$

$$\frac{\partial \mathbf{q_1}}{\partial t} + \frac{\partial[\mathbf{F_1} - \bar{\mathbf{F}}_\mathbf{1}]}{\partial x} + V_0 \frac{\partial \mathbf{q_1}}{\partial y} + \sigma_x \mathbf{q_1} + \sigma_x \beta_x [\mathbf{F_1} - \bar{\mathbf{F}}_\mathbf{1}] = 0 \tag{36}$$

A similar derivation leads to the y-layer equations:

$$\frac{\partial \mathbf{u}}{\partial t} + \frac{\partial[\mathbf{F_1} - \bar{\mathbf{F}}_\mathbf{1}]}{\partial x} + \frac{\partial[\mathbf{F_2} - \bar{\mathbf{F}}_\mathbf{2}]}{\partial y} + \sigma_y \mathbf{q_2} + \sigma_y \beta_y [\mathbf{F_2} - \bar{\mathbf{F}}_\mathbf{2}] = 0 \tag{37}$$

$$\frac{\partial \mathbf{q_2}}{\partial t} + U_0 \frac{\partial \mathbf{q_2}}{\partial x} + \frac{\partial[\mathbf{F_2} - \bar{\mathbf{F}}_\mathbf{2}]}{\partial y} + \sigma_y \mathbf{q_2} + \sigma_y \beta_y [\mathbf{F_2} - \bar{\mathbf{F}}_\mathbf{2}] = 0 \tag{38}$$

where

$$\beta_y = \frac{V_0}{1 - V_0^2} \tag{39}$$

Corner layers are again constructed based on a combination of equations (35)-(38). We want the corner layer equations to reduce automatically to the x- and y-layer equations when σ_y and σ_x are zero, respectively, and to be dynamically stable. These considerations lead to the following corner equations:

$$\frac{\partial \mathbf{u}}{\partial t} + \frac{\partial[\mathbf{F_1} - \bar{\mathbf{F}}_\mathbf{1}]}{\partial x} + \frac{\partial[\mathbf{F_2} - \bar{\mathbf{F}}_\mathbf{2}]}{\partial y} + \sigma_x \mathbf{q_1} + \sigma_y \mathbf{q_2} + \sigma_x \beta_x [\mathbf{F_1} - \bar{\mathbf{F}}_\mathbf{1}] + \sigma_y \beta_y [\mathbf{F_2} - \bar{\mathbf{F}}_\mathbf{2}] + \sigma_x \sigma_y (\mathbf{u} - \bar{\mathbf{u}}_\mathbf{p}) = 0 \tag{40}$$

$$\frac{\partial \mathbf{q_1}}{\partial t} + \frac{\partial[\mathbf{F_1} - \bar{\mathbf{F}}_\mathbf{1}]}{\partial x} + V_0 \frac{\partial \mathbf{q_1}}{\partial y} + (\sigma_x + \sigma_y)\mathbf{q_1} + \sigma_x \beta_x [\mathbf{F_1} - \bar{\mathbf{F}}_\mathbf{1}] = 0 \tag{41}$$

$$\frac{\partial \mathbf{q_2}}{\partial t} + U_0 \frac{\partial \mathbf{q_2}}{\partial x} + \frac{\partial[\mathbf{F_2} - \bar{\mathbf{F}}_\mathbf{2}]}{\partial y} + (\sigma_x + \sigma_y)\mathbf{q_2} + \sigma_y \beta_y [\mathbf{F_2} - \bar{\mathbf{F}}_\mathbf{2}] = 0 \tag{42}$$

A linear stability analysis has again been performed for (40)-(42). No instability mode is found, as is shown in Figures 5 and 6.

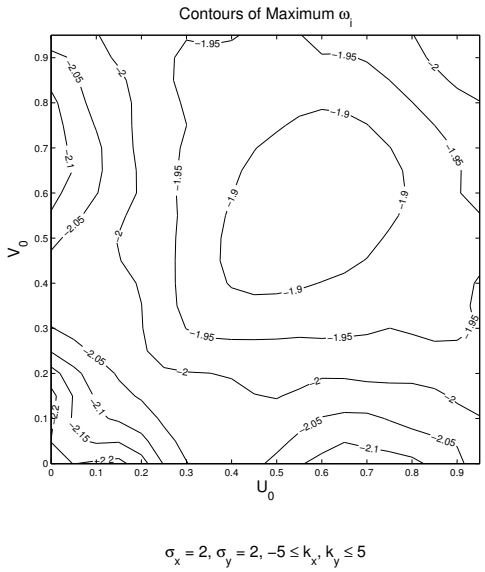

Figure 5. Contours of maximum imaginary part of ω for $\sigma_x = \sigma_y = 2.0$

V. Numerical Examples

A. Vorticity and entropy waves

To assess the performance of the proposed absorbing boundary condition (20)-(22) for the linearized Euler equation, we present a numerical example with oblique mean flow $(M_x, M_y) = (0.5, 0.5)$. The physical computational domain is $[-50, 50] \times [-50, 50]$ and is surrounded by absorbing layers of width D to absorb the outgoing waves. The equations are solved by a finite difference scheme with $\Delta x = \Delta y = 1$. The initial conditions for density ρ, velocity components u and v, and pressure p are

$$\rho = e^{-(ln2)\frac{x^2+y^2}{16}} + \sum_{n=1}^{3} e^{-(ln2)\frac{(x-x_n)^2+(y-y_n)^2}{16}}, \; p = e^{-(ln2)\frac{x^2+y^2}{16}} \tag{43}$$

$$u = \sum_{n=1}^{3} (y - y_n) e^{-(ln2)\frac{(x-x_n)^2+(y-y_n)^2}{16}}, \; v = -\sum_{n=1}^{3} (x - x_n) e^{-(ln2)\frac{(x-x_n)^2+(y-y_n)^2}{16}} \tag{44}$$

where $(x_1, y_1) = (25, 0)$, $(x_2, y_2) = \frac{\sqrt{2}}{2}(25, 25)$, and $(x_3, y_3) = (0, 25)$ are the initial locations of three vorticity and entropy pulses. The vorticity and entropy waves advect with the mean flow. As time progresses, two sets of the vorticity and entropy waves exit the top and right computational domain, while the third set exits at the upper right corner.

The absorption coefficient σ_x varies with space as

$$\sigma_x = 2 \left| \frac{x - x_0}{D} \right|^{\alpha} \tag{45}$$

where x_0 is the location of the Euler/PML interface. Similar functions are used for σ_y.

Figure 7 shows the contours of the density at $t = 0$, 70, 100 and 200. Since the numerical solution decays exponentially toward the edges of the PML domain, periodic boundary conditions are applied in this example. The absorption of waves inside the PML domain is observed in the contour plots. We also see that the reflection occurring at the corner is larger than that at the sides, because the corner layer is not perfectly matched, while the PML for x- and y-layers are. To assess the reflection error quantitatively, Figure 8 shows the maximum difference between the numerical solution and a reference solution obtained using a larger computational domain. The maximum difference for the density along $x = \pm 45$, $y = \pm 45$ is plotted as a function of time for given choices of PML width D and absorption coefficient power α. Clearly,

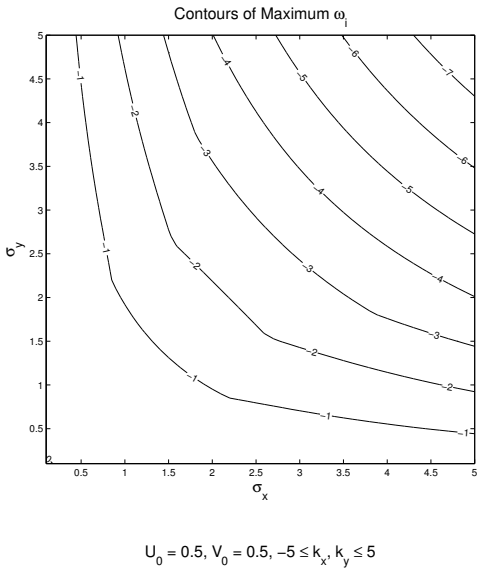

Figure 6. Contours of maximum imaginary part of ω for $U_0 = V_0 = 0.5$

the reflection error reduces as the width of the layer increases. A reflection error of less than 1% is achieved for density, pressure and velocity with a choice of $\alpha = 3$ and $D = 10\Delta x$.

B. Isentropic vortex

We will test the nonlinear PML equations (40)-(42) for a solution of the form

$$\begin{pmatrix} \rho(\mathbf{x},t) \\ u(\mathbf{x},t) \\ v(\mathbf{x},t) \\ p(\mathbf{x},t) \end{pmatrix} = \begin{pmatrix} 0 \\ U_0 \\ V_0 \\ 0 \end{pmatrix} + \begin{pmatrix} \rho_r(r) \\ -u_r(r)\sin\theta \\ u_r(r)\cos\theta \\ p_r(r) \end{pmatrix} \tag{46}$$

where $r = \sqrt{(x - U_0 t)^2 + (y - V_0 t)^2}$, and for a given $u_r(r)$ and $\rho_r(r)$, the pressure $p_r(r)$ is given by

$$\frac{d}{dr} p_r(r) = \rho_r(r) \frac{u_r^2(r)}{r} \tag{47}$$

This solution to the nonlinear Euler equations advects with constant velocity (U_0, V_0). For this example, we will assume a velocity distribution of the form

$$u_r(r) = \frac{U'_{max}}{b} r e^{\frac{1}{2}(1 - \frac{r^2}{b^2})} \tag{48}$$

where U'_{max} is the maximum velocity at $r = b$. For isentropic flow, we enforce the relationship

$$p_r = \frac{1}{\gamma} \rho_r^\gamma \tag{49}$$

which leads to the following density and pressure distributions

$$\rho_r(r) = \left(1 - \frac{1}{2}(\gamma - 1) U'^2_{max} e^{1 - \frac{r^2}{b^2}}\right)^{1/(\gamma - 1)} \tag{50}$$

$$p_r(r) = \frac{1}{\gamma} \left(1 - \frac{1}{2}(\gamma - 1) U'^2_{max} e^{1 - \frac{r^2}{b^2}}\right)^{\gamma/(\gamma - 1)} \tag{51}$$

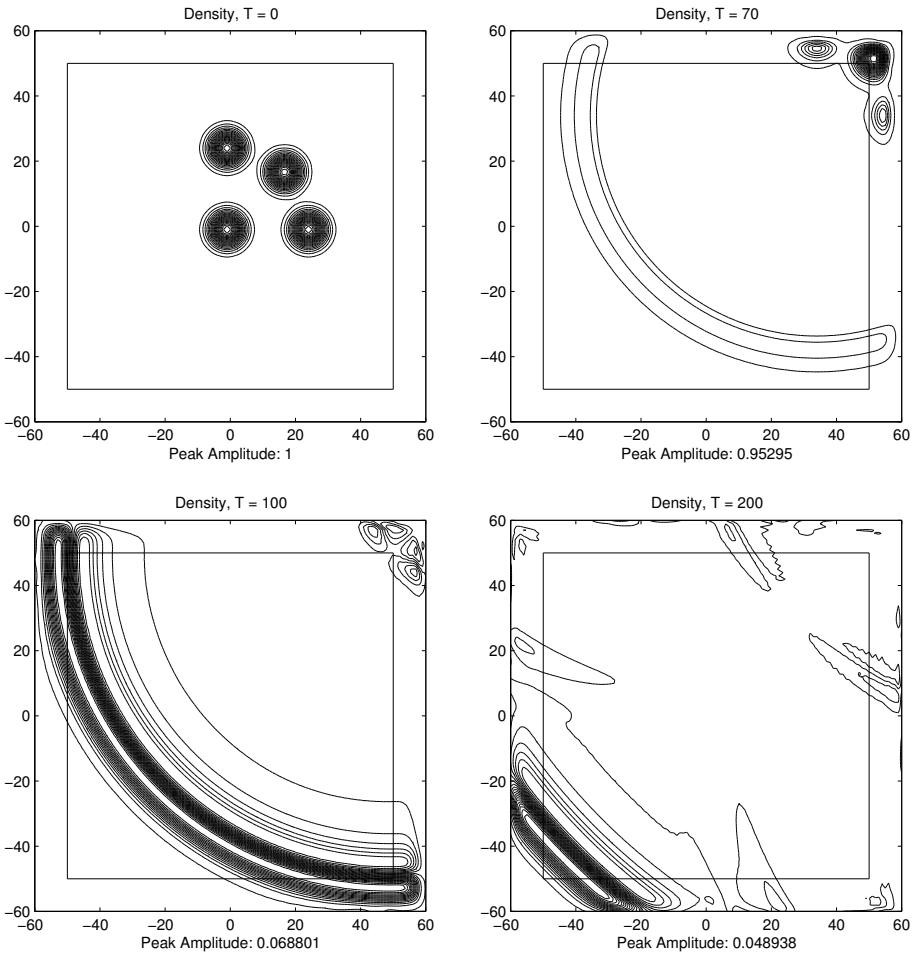

Figure 7. Contours of density at time t = 0, 70 , 100 and 200, showing three entropy waves and an acoustic wave located at the center. The mean flow Mach numbers are $M_x = M_y = 0.5$. $D = 10\Delta x$, $\alpha = 3$.

Figure 9 shows the contours of v-velocity at $t = 0$, 1.5, 2.0 and 2.5. Constant velocity was taken to be $(U_0, V_0) = (0.5, 0.5)$, and in the above distributions, $U'_{max} = 0.25$, $b = 0.2$, and $\gamma = 1.4$. The PML width was chosen to be 10 grid points, and the entire domain $[-1.2, 1.2]\times[-1.2, 1.2]$ was discretized by $\Delta x = \Delta y = 0.02$. For the PML absorption coefficients, σ_x and σ_y, parameter values $\sigma_{max} = 20$ and $\alpha = 4$ were chosen. To test the accuracy, numerical solutions were compared with reference solutions computed on the larger domain $[-6.2, 6.2] \times [-6.2, 6.2]$. Maximum difference between the numerical and reference solutions as a function of time was calculated along $x = \pm 0.9$ and $y = \pm 0.9$, shown in Figure 10.

Satisfactory results were also achieved for various cases of higher strength vortices. Taking $(U_0, V_0) = (0.2, 0.2)$, vortex strengths $U'_{max} = 1.2U_0, 1.4U_0, 1.6U_0, 1.8U_0$ were tested with good agreement between numerical and reference solutions. Error results are shown in Figure 11. In both cases, the background flow was taken as the uniform flow (U_0, V_0).

VI. Conclusions

PML absorbing boundary conditions for the linearized and nonlinear Euler equations have been derived in the form of x-, y-, and corner layer equations for the case of mean flow in an arbitrary direction. The x- and y-layer equations are perfectly matched, while the corner layer equations were shown to be stable. The proposed equations performed well in the given examples.

The capability of PML equations to absorb outgoing waves that exit the domain at an arbitrary angle is an important step in the movement toward modeling increasingly realistic aeroacoustic problems. Such

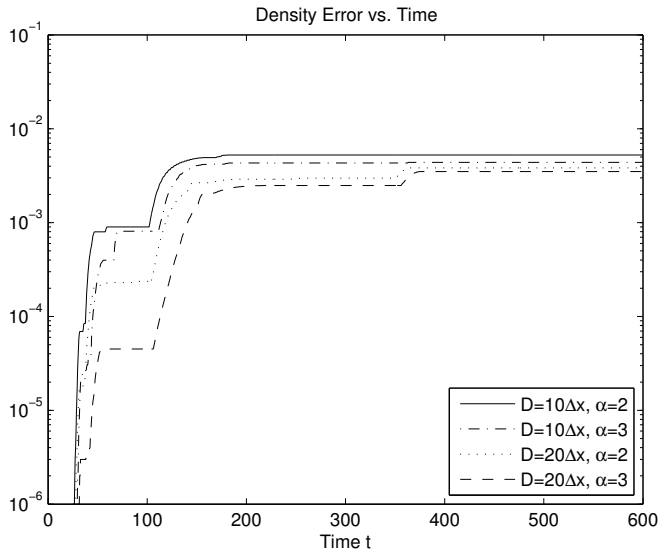

Figure 8. Maximum difference in density ρ between the numerical and reference solutions along $x = \pm 45$ and $y = \pm 45$.

capability will allow for a number of new configurations to be tested numerically.

Acknowledgments

This work is supported by a grant from the National Science Foundation DMS-0411402.

References

[1]Appelo, T. Hagstrom and G. Kreiss, "Perfectly matched layers for hyperbolic systems: General formulation, well-posedness and stability", SIAM J. Appl. Math., Vol. 67, 1-23, 2006

[2]E. Becache, S. Fauqueux and P. Joly, "Stability of perfectly matched layers, group velocities and anisotropic waves", Journal of Computational Physics, Vol. 188, 399-433, 2003.

[3]E. Becache, A.-S. Bonnet-Ben Dhia, G. Legendre, "Perfectly matched layers for the convective Helmholtz equation", SIAM J. Numerical Analysis, Vol. 42, 409-433, 2004.

[4]J.-P. Berenger, "A perfectly matched layer for the absorption of electromagnetic waves", Journal of Computational Physics, Vol. 114, 185-200, 1994.

[5]J. Diaz and P. Joly, "A time domain analysis of PML models in acoustics", Computational Methods in Applied Mechanics and Engineering, Vol. 195, 3820-3853, 2006.

[6]T. Hagstrom and I. Nazarov, "Absorbing layers and radiation boundary conditions for jet flow simulations", AIAA paper 2002-2606, 2002.

[7]T. Hagstrom and I. Nazarov, "Perfectly matched layers and radiation boundary conditions for shear flow calculations", AIAA paper 2003-3298, 2003.

[8]F. Q. Hu, "On absorbing boundary conditions for linearized Euler equations by a perfectly matched layer", Journal of Computational Physics, Vol. 129, 201-219, 1996.

[9]F. Q. Hu, "A stable, Perfectly Matched Layer for linearized Euler equations in unsplit physical variables", Journal of Computational Physics, Vol. 173, 455-480, 2001.

[10]F. Q. Hu, "A Perfectly Matched Layer absorbing boundary condition for linearized Euler equations with a non-uniform mean flow", Journal of Computational Physics, Vol 208, 469-492, 2005.

[11]F. Q. Hu, "On the construction of PML absorbing boundary condition for the non-linear Euler equations", AIAA paper 2006-0798, 2006.

[12]F. Q. Hu, X. D. Li and D. K. Lin, "PML absorbing boundary condition for non-linear aeroacoustics problems", AIAA paper 2006-2521, 2006.

[13]F. Nataf, "A new approach to perfectly matched layers for the linearized Euler system", Vol. 214, 757-772, 2006.

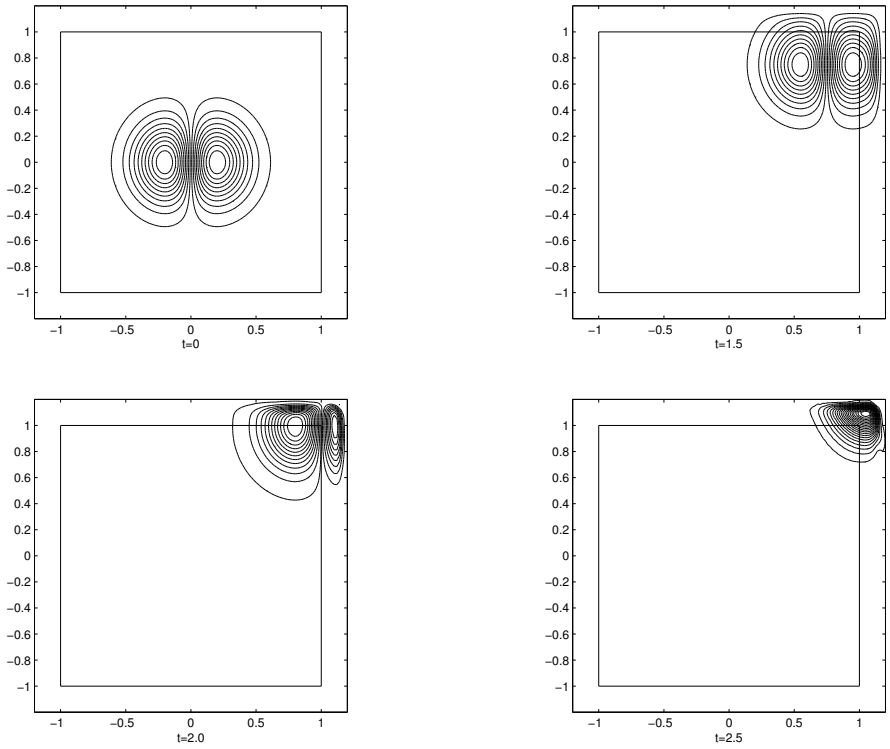

Figure 9. Contours of v-velocity

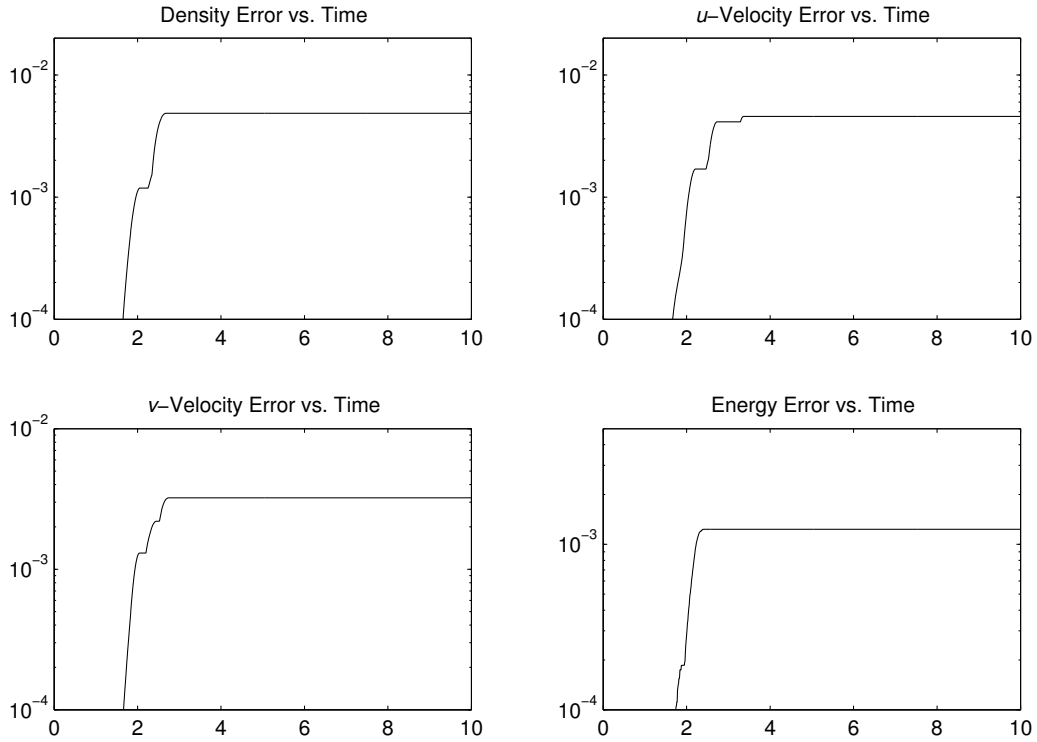

Figure 10. Maximum difference versus time along $x = \pm 0.9$, $y = \pm 0.9$ for $U_0 = V_0 = 0.5$, $U'_{max} = 0.25$.

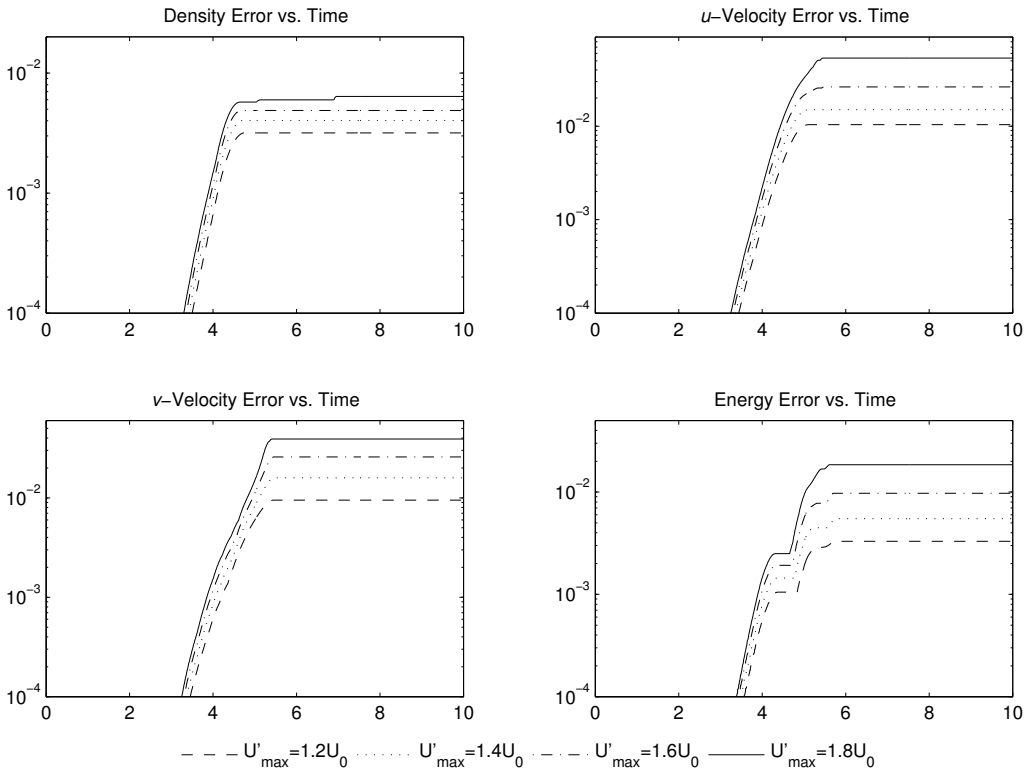

Figure 11. Maximum difference versus time along $x = \pm 0.9$, $y = \pm 0.9$ for $U_0 = V_0 = 0.2$ and varying U'_{max}.